Nanoscale

Accepted Manuscript

This article can be cited before page numbers have been issued, to do this please use: J. Zhou, Z. Li, M. Ying, M. Liu, X. Wang, X. Wang, L. Cao, H. Zhang and G. Xu, *Nanoscale*, 2018, DOI: 10.1039/C7NR08900G.

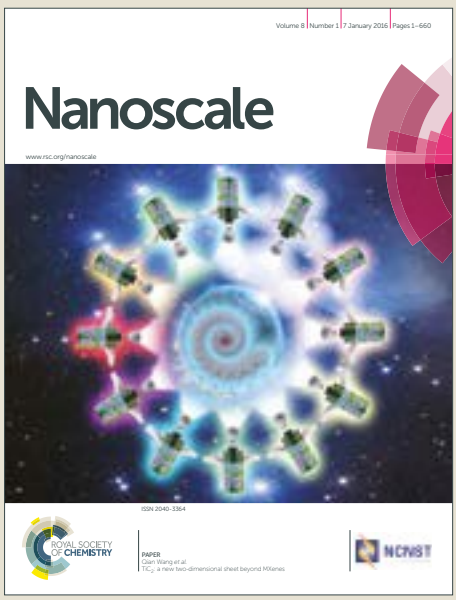

ROYAL SOCIETY OF CHEMISTRY

rsc.li/nanoscale

View Article Online
DOI: 10.1039/C7NR08900G

Nanoscale

COMMUNICATION

Black phosphorus nanosheets for rapid microRNA detection

Jie Zhou,[a] Zhongjun Li,[b] Ming Ying,[c] Maixian Liu,[a] Xiaomei Wang,[d] Xianyou Wang,[e] Liwei Cao,[e] Han Zhang [b]* and Gaixia Xu [a]*

Received 00th January 20xx,
Accepted 00th January 20xx

DOI: 10.1039/x0xx00000x

www.rsc.org/

Herein, for the first time, a sensitive sensing platform for rapid detection of microRNA was developed by employing black phosphorus nanosheets as fluorescence quenching material. The biosensor displayed a good linear response to microRNA ranging from 10 nM to 1000 nM. Moreover, the biosensor could distinguish triple nucleotide polymorphism.

MicroRNAs (miRNAs) are a group of ~22 nucleotide-long non-coding single-stranded RNA molecules encoded by endogenous genes. They are known to be involved in the regulation of post-transcriptional gene expression in plants and animals, which further regulate the growth, development and apoptosis process of organism[1]. In the field of medical research, altered expression patterns of miRNAs are associated with the development and progression of multiple diseases, for which miRNA is proposed as novel biomarkers for diseases diagnosis such as cancers[2], heart disease[3], diabetes[4] and neurogenic disorders[5]. Owing to the above features of miRNAs, the development of methods for miRNA detection has become a hot research field[6]. The most commonly used methodological approaches are the northern blot analysis[7], microarrays[8], real-time PCR[9] and high-throughput sequencing[10]. However, some of these methods are at the expense of quantitative determination, assay simplicity or rapid analysis time[6]. Therefore, it has been urgent to develop a simple and fast method of providing a quantitative measurement of miRNAs.

Two-dimensional(2D) nanomaterials have been widely used in the field of biomolecule sensing for their outstanding chemical and physical properties[11]. The exploration started with graphene[12], a kind of single-atom thick 2D carbon nanomaterial, and its related nanomaterial such as graphene oxide[13] and graphene quantum dots[14]. More recently, graphene-like 2D layered nanomaterials (GLNs), including boron nitride nanosheets, graphitic-carbon nitride nanosheets and transition metal dichalcogenides or dioxides (TMDs, e.g. MoS_2 and WS_2) have attracted significant interest in numerous research fields from physics and chemistry to biosensing and nanomedicine[15]. As for miRNA sensing, many researchers have demonstrated the applicability of graphene and GLNs as biomolecule labels[16, 17] and electrode surface[18, 19]. In addition, graphene and GLNs have also been utilized as either fluorophores[20] or quenchers[21, 22] in the detection of nucleic acid, just like other nanomaterials[23-26].

Among the large family of 2D nanomaterial, black phosphorus nanosheets (BPNSs) have sparked growing interests in material science since they were first exfoliated from bulk black phosphorus in 2014[27]. BP has distinct structure with corrugated planes of phosphorus (P) atoms, which are connected by strong intralayer P-P bonding and weak interlayer van der Waals forces[28]. BPNSs owns many similar properties with other 2D nanomaterials while offers its unique properties such as a high carrier mobility, high transport anisotropy and layer-dependent bandgap[29]. These properties have made BPNSs a promising candidate in electronics, optoelectronics, and thermoelectric application[29]. Besides, BPNSs exhibit better biocompatibility and biosafety as phosphorus is an essential element for maintaining good health in humans, indicating that BPNSs hold great promise as a novel nanomaterial for biomedical applications[28, 30]. BPNSs has also been applied in the analytical sciences[31]. Initially, BPNSs was used to fabricate gas and vapor sensors [32]. Later, researchers have utilized BPNSs to detect a variety of analytes including hydrogen peroxide[33], inorganic ions[34] and disease

[a] Key Laboratory of Optoelectronics Devices and Systems of Ministry of Education/Guangdong Province, College of Optoelectronic Engineering, Shenzhen University, Shenzhen 518060, China.
[b] Shenzhen Engineering Laboratory of Phosphorene and Optoelectronics, SZU-NUS Collaborative Innovation Center for Optoelectronic Science and Technology, and Key Laboratory of Optoelectronic Devices and Systems of Ministry of Education and Guangdong Province, Shenzhen University, Shenzhen 518060, China
[c] College of Life Sciences, Shenzhen Key Laboratory of Marine Bioresources and Ecology/Shen Zhen Key Laboratory of Microbial Genetic Engineering, Shenzhen University, Shenzhen 518060, China
[d] Department of Physiology, School of Basic Medical Sciences, Shenzhen University Health Sciences Center, Shenzhen 518060, China.
[e] Nanophotonics Research Centre, Shenzhen University, Shenzhen 518060, China
*Corresponding Authors: Gaixia Xu: xugaixia@szu.edu.cn; Han Zhang: hzhang@szu.edu.cn
Electronic Supplementary Information (ESI) available: [details of any supplementary information available should be included here]. See DOI: 10.1039/x0xx00000x

View Article Online
DOI: 10.1039/C7NR08900G

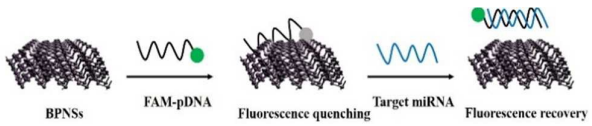

Scheme 1 Schematic illustration of BPNSs-based fluorescent miRNA sensing platform

biomarkers[35] in electrochemical, electrical, and fluorescence transducing modes. Recently, Ying et al. utilized the capacity of BPNSs in discriminating single-stranded DNA (ssDNA) and double-stranded DNA (dsDNA) for sensitive DNA detection, which inspired our research[36].

In this study, we presented the application of BPNSs as fluorescence quenching material to develop a novel biosensor for rapid and sensitive miRNA detection. To the best of our knowledge, this is the first literature that explores BPNSs in the analysis of miRNA because of its capacity of DNA adsorbing and fluorescence quenching. This work provides a new strategy to fabricate BPNSs as promising nanostructure for biomolecule detection.

Scheme 1 illustrates the schematic representation of miRNA sensing platform. Firstly, 6-Carboxyfluorescein (6-FAM)-labelled ssDNA probes (pDNA) were adsorbed on the BPNSs surface via Van der Waals force between nucleobases and the P atoms of BPNSs. The close proximity of pDNA and BPNSs facilitated the fluorescence resonance energy transfer (FRET) from FAM to BPNSs, which resulted in fluorescence quenching of FAM. After the addition of target miRNA, the pDNA formed a duplex with the complementary miRNA strand by hybridization. Then the affinity of BPNSs for pDNA was reduced, leading to the release of pDNA from BPNSs. Consequently, the fluorescence of pDNA was recovered.

Initially, BPNSs were synthesized from bulk BP crystal by liquid exfoliation in N-methyl-2-pyrrolidone (NMP) (Fig. S1, ESI†). Atomic force microscope (AFM), transmission electron microscopy (TEM), hydrodynamic size analysis and Raman spectroscopy were carried out to characterize the structure of the BPNSs. The AFM image shows the topographic morphology of BPNSs (Fig. 1a). The heights of BPNSs labelled with line 1, line 2 and line 3 are measured to be 30, 15, and 7.5 nm (Fig. 1b). Statistical AFM analysis gives an average thickness of 18.4±1.5 nm (Fig. S2, ESI†), that is, the average layer numbers of BPNSs are about 35±3, considering that the thickness of mono-layer phosphorene is 0.53 nm[37]. The TEM analysis of the BPNSs clearly shows that the nanosheets have length in the range of few hundreds nanometres with stacked folds and varying thickness (Fig. 1c). Moreover, the high-resolution TEM (HRTEM) image of BPNSs displays lattice fringes of 0.217 nm, which can be ascribed to the (002) planes of black phosphorous (Fig. S3, ESI†). In addition, the result of hydrodynamic size analysis indicates that the average diameter of BPNSs is 298.4±6.7 nm (Fig. S4, ESI†).The Raman scattering spectrum of exfoliated BPNSs depicts three identical Raman peaks located at ≈363.6, 441, and 469 cm^{-1} (Fig. 1d), which correspond to A^1_g, B_{2g}, and A^2_g modes of BPNSs and coincide with those reported in the literature[32, 38]. Furthermore, the crystal structure of BPNSs was determined by XRD, and Fig. S5 shows the reflective patterned peaks at 2θ= 16.78°, 34.03° and 52.18°, which are attributed to the

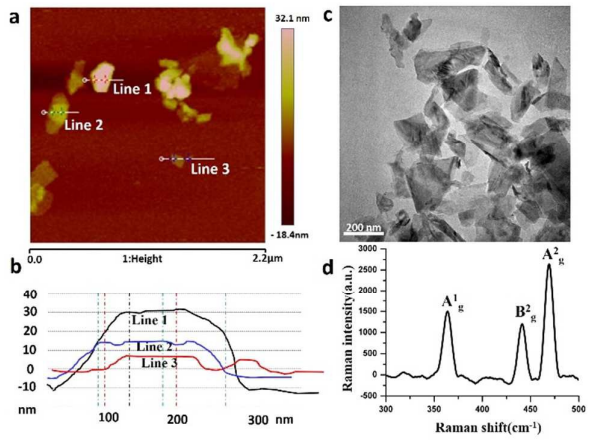

Fig. 1 (a) AFM image of BPNSs. (b) Height profiles of BPNSs. The heights of BPNSs labelled with line 1, line 2 and line 3 are measured to be 30, 15, and 7.5 nm (c) TEM image of prepared BPNSs. Scale bar: 200 nm. The BPNSs have length in the range of few hundreds nanometres with stacked folds and varying thickness. (D) The Raman spectrum of BPNSs. The Raman scattering spectrum of exfoliated BPNSs depicts three identical Raman peaks located at ≈363.6, 441, and 469 cm^{-1}, which correspond to A^1_g, B^2_g, and A^2_g modes of BPNSs.

(020), (040), (060) diffractions, respectively, and is consistent with that of standard orthorhombic black phosphorus (JCPDS No.73-1358).

Similar to other 2D layered nanostructures such as graphene oxide[39] and WS_2[40], BPNSs exhibit a broad absorption band from the UV region to the NIR region (Fig. S6a, ESI†). A perfect linear trend is observed for the absorbance at wavelength λ=520 nm versus the concentration of BPNSs, indicating that the absorbance at λ=520 nm can be used to determine the concentration of BPNSs (Fig. S6b, ESI†). The extinction coefficient of BPNSs at 520 nm is calculated to be 62 L/(g*cm), according to the Lambert- Beer law, A/L=α*C. Compared with previously reported 2D layered materials, the extinction coefficient of BPNSs at λ=520 nm is much higher than that of GO (14.4 L/(g*cm)) and reduced GO (32 L/(g*cm))[39] and comparable to that of WS_2 nanosheets (63.3 L/(g*cm))[40]. Considering the emission wavelength of FAM is 520 nm, BPNSs might be a good candidate for FAM quenching.

To demonstrate the working principle of our sensing platform, the typical emission spectral responses of pDNA at different conditions were measured. Oligonucleotide

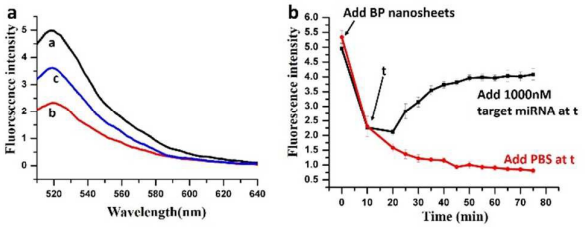

Fig. 2 (a) The emission spectral response of pDNA (curve a), after the addition of BPNSs (curve b) and target miRNA (curve c). (B) The fluorescence intensity at λ=520 nm of pDNA-BPNSs complex with PBS or 1000 nM target miRNA as a function of time. The curves represent the average values of three wells with error bars showing the standard deviation of three wells at each time points.

View Article Online
DOI: 10.1039/C7NR08900G

sequences are as follows: pDNA is 5' 6-FAM TCA TAG CCC TGT ACA ATG CTG CT 3' and the complementary target miRNA hsa-miR-103a-3p: 5' AGC AGC AUU GUA CAG GGC UAU GA 3'. Hsa-miR-103a-3p was reported to be downregulated in the plasma of Alzheimer disease patients. In the absence of BPNSs, the fluorescence spectrum of pDNA shows relatively strong fluorescence emission with a peak at λ=520 nm owing to the presence of labelled FAM (Fig. 2a, curve a). However, the fluorescence intensity is greatly reduced after BPNSs is added in the solution, indicating the strong adsorption of the pDNA on BPNSs and effective fluorescence quenching by BPNSs (Fig. 2a, curve b). While, upon the addition of complementary target miRNA to the pDNA-BPNSs mixture, the solution shows obvious fluorescence restoration (Fig. 2a, curve c). This implies that the distance between pDNA and BPNSs become larger after hybridization, which prevented the FRET process between them.

The kinetic behaviours of pDNA-BPNSs complex with PBS and 1000 nM target miRNA were studied by monitoring the fluorescence intensity at λ=520 nm as a function of time. The fluorescence intensity continues to increase as more and more absorbed pDNA hybridize with target miRNA and release from BPNSs (Fig. 2b). The intensity reaches equilibrium at 30 minutes after 1000 nM target miRNA is added into wells. And the intensity is restored to 70% of initial intensity. Thus, incubation time of 30 minutes was used as optimized detection time. As a result, the total measurement duration is about 40 minutes. While the fluorescence intensity decreases slowly after PBS is added into wells since pDNA kept absorbed on BPNSs. The adsorption was saturated at 30 minutes.

We carried out molecular dynamics (MD) simulation to interrogate the observed difference between the affinity of ssDNA and DNA/RNA duplex for single layer BPNS. As shown in the final snapshot of the MD simulation (Fig. 3a), the nucleobases lie flat at the basal plane, and the ssDNA is stably adsorbed by BPNS. This adsorption is mainly due to van der Waals interactions between the P atoms in BPNS and the carbon/oxygen/nitrogen atoms of nucleobases since the final average distance between nucleobases and the BPNS is less than 5A˚(Fig. 3c). While DNA/RNA duplex maintains its helical structure and is floated on the plane of BPNS (Fig. 3b). This is because nucleobases form base pairs by hydrogen bonds and are shielded within the phosphate backbone of DNA/RNA duplex. Fig.3c also indicates the average distance between DNA bases in DNA/RNA duplex and the BPNS is larger than 1.2 nm (the cut-off radius of non-bonded interaction), which means rarely van der Waals interactions between the atoms of nucleobases and P atoms of BPNS. Consequently, the distance between FAM and the BPNS increases significantly, thus inducing the fluorescence recovery of FAM. The interactions process between BPNS and ssDNA, and that between BPNS and DNA/RNA duplex have been demonstrated in the video provided in the ESI 2 and ESI 3, respectively.

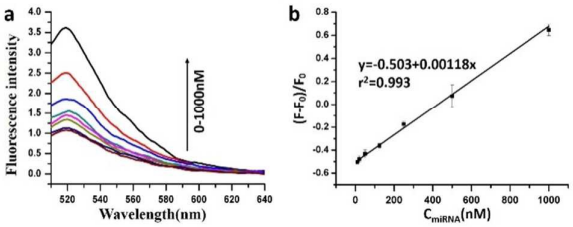

Fig. 4 (a) The fluorescence emission spectra of pDNA-BPNSs complex after incubating with varying concentration of target miRNA at 0, 10, 20, 50, 125, 250, 500, 1000 nM for 30min. (b) The calibration curve of △F versus C_{miRNA}(10-1000 nM). The curves represent the average values of three wells with error bars showing the standard deviation of three wells at each concentration.

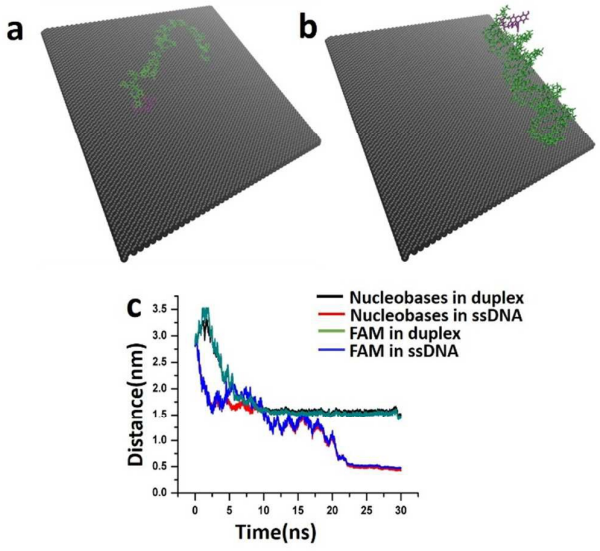

Fig. 3 The final snapshots of the MD simulation showing the difference between the affinity of a) ssDNA and b) DNA/RNA duplex for single layer BPNS. The FAM, nucleic acids and BPNS are shown in purple, green and black, respectively. c) The average distance between nucleobases in ssDNA, nucleobases in duplex, FAM in ssDNA, FAM in duplex and the BPNS plane as a function of simulation time.

Next, we evaluated the dynamic range and sensitivity of the miRNA sensing platform. Under optimal condition (Fig. S7, ESI†), pDNA (25 nM) was interacted with BPNSs (200 μg/ml) for 10 minutes; then different concentrations of target miRNA (0 to 1000 nM) were added and incubated for 30 minutes. Fig. 4a shows the fluorescence emission spectra of pDNA-BPNSs complex after incubating with different concentration of target miRNA for 30 minutes. As depicted from Fig. 4a, the

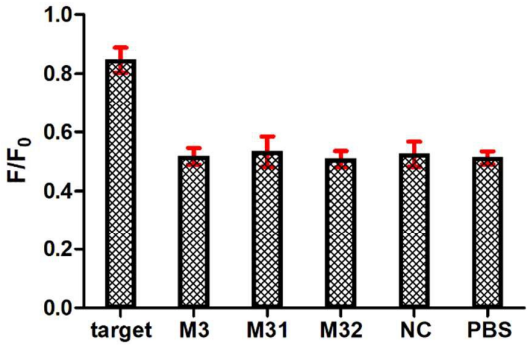

Fig. 5 Specificity of miRNA assay. Bars represent the fluorescence intensity ratio (F/F_0, F_0 is the fluorescence intensity of pDNA-BPNSs complex at λ=520 nm before miRNA was added into wells, F is the fluorescence intensity of pDNA-BPNSs complex at λ=520 nm after incubating with different miRNA for 30 min) upon the addition of target miRNA, M3, M31, M32, NC and PBS with the same concentration of 250 nM. The error bars represent the standard deviation of three wells under same condition.

View Article Online
DOI: 10.1039/C7NR08900G

fluorescence emission intensity increases gradually with the increasing concentration of target miRNA, indicating the fluorescence recovery by target miRNA.

The calibration curve of ΔF (ΔF=F/F_0-1, F_0 is the fluorescence intensity of pDNA-BPNSs complex at λ=520 nm before target miRNA was added into wells, F is the fluorescence intensity of pDNA-BPNSs complex at λ=520 nm after incubating with different concentration of target miRNA for 30 minutes) versus C_{miRNA} is given in Fig. 4b, which exhibits a linear region in the concentration range of 10 nM-1000 nM. The linear regression equation is ΔF = -0.50314+0.00118C_{miRNA} (nM, r^2 = 0.993). And the detection limit is 9.37 nM as estimated according to the 3σ rule. The linear dependence of ΔF on the miRNA concentration indicates that this method is suitable for quantitative analysis of miRNA. The detection range of this assay is wider than that of the GO-based fluorescent assay[41]. Besides, it should be noticed that by using multimode microplate reader and 96-well plate, the detection could be more simple, economical, efficient and accurate with smaller factitious operation errors.

The specificity of the biosensor was also tested by examining the fluorescence intensity ratio (F/F_0) of pDNA-BPNSs mixture toward target miRNA, three-base mismatched miRNA (M3, M31, M32) and non-complementary miRNA (NC). The Oligonucleotide sequences of M3, M31, M32 and NC are as follows: M3 is 5' AGC AGC **U**UU GU**G** CAG GGC UAU **C**A 3', M31: 5' **UAG** AGC AUU GUA CAG GGC UAU GA 3', M32: 5' AGC AGC AUU GUA CAG GGC UA**G AG** 3', and the NC: 5' UUG UAC UAC ACA AAA GUA CUG 3'. As shown in fig.5, the F/F_0 values obtained upon the incubation of 250 nM target miRNA, M3, M31, M32, NC and PBS are 0.846, 0.517, 0.533, 0.507, 0.524, and 0.512, respectively. The fluorescence intensity ratio of M3 M31, M32, and NC group don't show obvious difference compared with that of PBS group, which demonstrated that the biosensor could distinguish target miRNA from three-base mismatched or non-complementary miRNA. The results illustrates that the biosensor has the ability to discriminate three-nucleotide-length polymorphisms.

Conclusions

In this study, for the first time, we utilized BPNSs as a novel nanomaterial in the development of a fluorescence-based biosensor for simple, fast and sensitive miRNA detection. The BPNSs were prepared by liquid exfoliation route with few hundred manometers in size and average thickness of 18.4±1.5 nm. By employing BPNSs as fluorescence quenching material, the biosensor had a linear range of 10-1000 nM, with a detection limit of 9.37 nM under a simple experimental procedure and relatively short detection time (40 minutes). Meanwhile, the biosensor showed acceptable specificity. In addition, we used molecular dynamics (MD) simulation to explicate the difference between the interaction of ssDNA and DNA/RNA duplex with BPNSs, which demonstrated the detection principle of the biosensor. What's more important, the robustness of the biosensor allows for the measuring of other targets including DNAs, proteins and inorganic ions as long as the nucleotide sequence of probes is elaborately designed. It is therefore envisaged that our research opens up the investigations and application of BPNPs in fluorescence quenching-based biosensing for biomedical research and clinical diagnostics.

Acknowledgements

This article was prepared with support from the National Natural Science Foundation of China (31671491, 61335001, 61527827 and 61775148), National Basic Research Program of China (2015CB352005), Guangdong Natural Science Foundation (2014A030312008&2017B020210006), Shenzhen Science and Technology R&D and Innovation Foundation (JCYJ20160422151611496, GRCK2017042110420047), China Scholarship Council (CSC) and Chinese Postdoctoral Science Foundation (2016M602523).

Conflicts of interest

There are no conflicts to declare.

Notes and references

1. N. Bushati and S. M. Cohen, *Annual Review of Cell and Developmental Biology*, 2007, **23**, 175-205.
2. M. V. Iorio and C. M. Croce, *Embo Molecular Medicine*, 2012, **4**, 143-159.
3. T. Thum and M. Mayr, *Cardiovascular Research*, 2012, **93**, 543-544.
4. C. Guay and R. Regazzi, *Nature Reviews Endocrinology*, 2013, **9**, 513-521.
5. M. Christensen and G. M. Schratt, *Neuroscience Letters*, 2009, **466**, 55-62.
6. M. D. Planell-Saguer and M. C. Rodicio, *Analytica Chimica Acta*, 2011, **699**, 134-152.
7. K. S. Woo, Z. Li, P. S. Moore, M. A. Paula, Y. Chang, N. Mark and J. Bino, *Nucleic Acids Research*, 2010, **38**, e98-e98.
8. D. K. Lv, X. Bai, Y. Li, X. D. Ding, Y. Ge, H. Cai, W. Ji, N. Wu and Y. M. Zhu, *Gene*, 2010, **459**, 39-47.
9. E. M. Kroh, R. K. Parkin, P. S. Mitchell and M. Tewari, *Methods*, 2010, **50**, 298-301.
10. E. Zhu, F. Zhao, G. Xu, H. Hou, L. Zhou, X. Li, Z. Sun and J. Wu, *Nucleic acids research*, 2010, **38**, W392-W397.
11. D. Chimene, D. L. Alge and A. K. Gaharwar, *Advanced Materials*, 2015, **27**, 7261-7284.
12. V. Georgakilas, J. N. Tiwari, K. C. Kemp, J. A. Perman, A. B. Bourlinos, K. S. Kim and R. Zboril, *Chemical Reviews*, 2016, **116**, 5464.
13. D. Sharma, S. Kanchi, M. I. Sabela and K. Bisetty, *Arabian Journal of Chemistry*, 2016, **9**, 238-261.
14. J. Shen, Y. Zhu, X. Yang and C. Li, *Chemical communications*, 2012, **48**, 3686-3699.
15. G. Yang, C. Zhu, D. Du, J. Zhu and Y. Lin, *Nanoscale*, 2015, **7**, 14217-14231.
16. Q. Wang, Q. Li, X. Yang, K. Wang, S. Du, H. Zhang and Y. Nie, *Biosensors & Bioelectronics*, 2016, **77**, 1001.

View Article Online
DOI: 10.1039/C7NR08900G

17. S. Su, W. Cao, W. Liu, Z. Lu, D. Zhu, J. Chao, L. Weng, L. Wang, C. Fan and L. Wang, *Biosensors & Bioelectronics*, 2017, **94**, 552-559.
18. X. Wu, Y. Chai, R. Yuan, Y. Zhuo and Y. Chen, *Sensors & Actuators B Chemical*, 2014, **203**, 296-302.
19. Q.-M. Feng, Y.-Z. Shen, M.-X. Li, Z.-L. Zhang, W. Zhao, J.-J. Xu and H.-Y. Chen, *Analytical chemistry*, 2015, **88**, 937-944.
20. H. Zhang, Y. Wang, D. Zhao, D. Zeng, J. Xia, A. Aldalbahi, C. Wang, L. San, C. Fan, X. Zuo and X. Mi, *ACS Applied Materials & Interfaces*, 2015, **7**, 16152-16156.
21. Z. Lu, L. Zhang, Y. Deng, S. Li and N. He, *Nanoscale*, 2012, **4**, 5840-5842.
22. Q. Xi, D. M. Zhou, Y. Y. Kan, J. Ge, Z. K. Wu, R. Q. Yu and J. H. Jiang, *Analytical Chemistry*, 2014, **86**, 1361-1365.
23. H. Li, Y. Zhang, Y. Luo and X. Sun, *Small*, 2011, **7**, 1562-1568.
24. L. Yang, D. Liu, S. Hao, F. Qu, R. Ge, Y. Ma, G. Du, A. M. Asiri, L. Chen and X. Sun, *Analytical Chemistry*, 2017, **89**, 2191-2195.
25. Y. Zhang, L. Wang, J. Tian, H. Li, Y. Luo and X. Sun, *Langmuir*, 2011, **27**, 2170-2175.
26. L. Wang, Y. Zhang, J. Tian, H. Li and X. Sun, *Nucleic Acids Research*, 2011, **39**, 1-6.
27. V. Eswaraiah, Q. Zeng, Y. Long and Z. Liu, *Small*, 2016, **12**, 3480-3502.
28. W. Tao, X. Zhu, X. Yu, X. Zeng, Q. Xiao, X. Zhang, X. Ji, X. Wang, J. Shi and H. Zhang, *Advanced Materials*, 2017, **29**.
29. Y. Zhao, Y. Chen, Y. H. Zhang and S. F. Liu, *Materials Chemistry & Physics*, 2017, **189**, 215-229.
30. Z. Sun, H. Xie, S. Tang, X. Yu, Z. Guo, J. Shao, H. Zhang, H. Huang, H. Wang and P. K. Chu, *Angewandte Chemie*, 2015, **127**, 11688-11692.
31. M. Pumera, *Trac Trends in Analytical Chemistry*, 2017, **93**, 1-6.
32. C. C. Mayorga‐Martinez, Z. Sofer and M. Pumera, *Angewandte Chemie*, 2015, **127**, 14525-14528.
33. S. Yan, B. Wang, Z. Wang, D. Hu, X. Xu, J. Wang and Y. Shi, *Biosensors & Bioelectronics*, 2016, **80**, 34.
34. W. Gu, X. Pei, Y. Cheng, C. Zhang, J. Zhang, Y. Yan, C. Ding and Y. Xian, 2017.
35. P. Jian, Y. Lai, Y. Chen, J. Xu, L. Sun and W. Jian, *Small*, 2017, **13**, 1-11.
36. T. Y. Ying, Z. Sofer, C. C. Mayorgamartinez and M. Pumera, *Materials Chemistry Frontiers*, 2017.
37. X. Wang, A. M. Jones, K. L. Seyler, V. Tran, Y. Jia, H. Zhao, H. Wang, L. Yang, X. Xu and F. Xia, *Nature nanotechnology*, 2015, **10**, 517-521.
38. D. J. Late, *Microporous and Mesoporous Materials*, 2016, **225**, 494-503.
39. J. T. Robinson, S. M. Tabakman, Y. Liang, H. Wang, H. Sanchez Casalongue, D. Vinh and H. Dai, *Journal of the American Chemical Society*, 2011, **133**, 6825-6831.
40. L. Cheng, J. Liu, X. Gu, H. Gong, X. Shi, T. Liu, C. Wang, X. Wang, G. Liu and H. Xing, *Advanced materials*, 2014, **26**, 1886-1893.
41. S. He, B. Song, D. Li, C. Zhu, W. Qi, Y. Wen, L. Wang, S. Song, H. Fang and C. Fan, *Advanced Functional Materials*, 2010, **20**, 453–459.